



Publication Year	2018
Acceptance in OA@INAF	2020-10-23T12:16:21Z
Title	þ Star Formation Histories of z = 1 Galaxies in LEGA-C
Authors	Chauke, Priscilla; VAN DER WEL, ARJEN; Pacifici, Camilla; Bezanson, Rachel; Wu, Po-Feng; et al.
DOI	10.3847/1538-4357/aac324
Handle	http://hdl.handle.net/20.500.12386/27959
Journal	THE ASTROPHYSICAL JOURNAL
Number	861



Star Formation Histories of $z \sim 1$ Galaxies in LEGA-C

Priscilla Chauke¹, Arjen van der Wel^{1,2}, Camilla Pacifici³, Rachel Bezanson⁴, Po-Feng Wu¹, Anna Gallazzi⁵, Kai Noeske⁶, Caroline Straatman², Juan-Carlos Muños-Mateos⁷, Marijn Franx⁸, Ivana Barišić⁹, Eric F. Bell¹⁰, Gabriel B. Brammer³, Joao Calhau¹¹, Josha van Houdt⁹, Ivo Labbé⁸, Michael V. Maseda⁸, Adam Muzzin¹², Hans-Walter Rix⁹, and David Sobral^{8,11}

¹ Max-Planck-Institut für Astronomie, Königstuhl 17, D-69117 Heidelberg, Germany; chauke@mpia-hd.mpg.de

² Sterrenkundig Observatorium, Universiteit Gent, Krijgslaan 281 S9, B-9000 Gent, Belgium

³ Space Telescope Science Institute, 3700 San Martin Drive, Baltimore, MD 21218, USA

⁴ University of Pittsburgh, Department of Physics and Astronomy, 100 Allen Hall, 3941 O'Hara Street, Pittsburgh PA 15260, USA

⁵ INAF-Osservatorio Astrofisico di Arcetri, Largo Enrico, Fermi 5, I-50125 Firenze, Italy

⁶ Experimenta Heilbronn, Kranenstraße 14, D-74072 Heilbronn, Germany

⁷ European Southern Observatory, Alonso de Cordova 3107, Casilla 19001, Vitacura, Santiago, Chile

⁸ Leiden Observatory, Leiden University, P.O. Box 9513, 2300 RA Leiden, The Netherlands

⁹ Max-Planck Institut für Astronomie, Königstuhl 17, D-69117 Heidelberg, Germany

¹⁰ Department of Astronomy, University of Michigan, 1085 S. University Avenue, Ann Arbor, MI 48109, USA

¹¹ Physics Department, Lancaster University, Lancaster LA1 4 YB, UK

¹² Department of Physics and Astronomy, York University, 4700 Keele Street, Toronto, ON M3J 1P3, Canada

Received 2017 December 13; revised 2018 April 20; accepted 2018 May 6; published 2018 June 26

Abstract

Using high-resolution spectra from the VLT Large Early Galaxy Astrophysics Census (LEGA-C) program, we reconstruct the star formation histories (SFHs) of 607 galaxies at redshifts $z = 0.6\text{--}1.0$ and stellar masses $\gtrsim 10^{10} M_{\odot}$ using a custom full spectrum fitting algorithm that incorporates the *emcee* and FSPS packages. We show that the mass-weighted age of a galaxy correlates strongly with stellar velocity dispersion (σ_*) and ongoing star formation (SF) activity, with the stellar content in higher- σ_* galaxies having formed earlier and faster. The SFHs of quiescent galaxies are generally consistent with passive evolution since their main SF epoch, but a minority show clear evidence of a rejuvenation event in their recent past. The mean age of stars in galaxies that are star-forming is generally significantly younger, with SF peaking after $z < 1.5$ for almost all star-forming galaxies in the sample: many of these still have either constant or rising SFRs on timescales > 100 Myr. This indicates that $z > 2$ progenitors of $z \sim 1$ star-forming galaxies are generally far less massive. Finally, despite considerable variance in the individual SFHs, we show that the current SF activity of massive galaxies ($> L_*$) at $z \sim 1$ correlates with SF levels at least 3 Gyr prior: SFHs retain “memory” on a large fraction of the Hubble time. Our results illustrate a novel approach to resolve the formation phase of galaxies, and, by identifying their individual evolutionary paths, one can connect progenitors and descendants across cosmic time. This is uniquely enabled by the high-quality continuum spectroscopy provided by the LEGA-C survey.

Key words: galaxies: evolution – galaxies: high-redshift – galaxies: star formation – galaxies: stellar content

1. Introduction

The ability to reconstruct the star formation histories (SFHs) of galaxies, by characterizing their stellar populations, allows one to trace their individual evolution through time, and thereby directly connect their descendants to their progenitors at higher redshifts. Thus far, high-redshift galaxy surveys have produced snapshots of the galaxy population at different points in cosmic time, which produces tight boundary conditions for galaxy formation models. However, the importance of the many physical processes included in these models are not directly constrained. We still do not know individual SFHs and how they are related to global galaxy properties. To constrain galaxy formation theories more directly, “archaeological” reconstruction can be used to trace the evolution of individual galaxies over time, and then the dependence of individual SFHs on stellar mass, stellar velocity dispersion, and star formation (SF) activity can be explored.

Reconstructing SFHs requires high-resolution spectra of galaxies. Ideally, individual stars would be resolved, as they are for local dwarf galaxies (e.g., Weisz et al. 2011). However, in most cases, we have to rely on integrated stellar light, though if a galaxy’s main SF epoch lies at $z > 1$, we cannot temporally

resolve its stellar age distribution, even with the highest-quality spectra. While there is a plethora of high-resolution spectra of galaxies in the local universe, most of these galaxies are too old (> 5 Gyr, Gallazzi et al. 2005) to resolve their SFHs due to the similarity of stellar spectra in the age range > 5 Gyr. The general insight gained from the “archaeological” studies of these galaxies is that low-mass galaxies have more extended SFHs that peak at later cosmic times compared to high-mass galaxies (“downsizing,” e.g., Gallazzi et al. 2005; Thomas et al. 2005, 2010). Many of these studies involved the use of fossil record methods on the Sloan Digital Sky Survey (SDSS, York et al. 2000) spectra of local galaxies (e.g., Juneau et al. 2005; Thomas et al. 2005; Cid Fernandes et al. 2007; Tojeiro et al. 2009; McDermid et al. 2015; Ibarra-Medel et al. 2016). However, downsizing has also been seen in other studies, such as studies by Cimatti et al. (2006), who corrected luminosity function data of early-type galaxies by adopting the empirical luminosity dimming rate derived from the evolution of the Fundamental Plane of field and cluster massive early-type galaxies, as well as Leitner (2012), who derived the average growth of stellar mass in local star-forming galaxies using a Main Sequence Integration approach.

One approach to probe the high-redshift regime, is to obtain an integrated view of galaxy evolution. Thus far, this has been the focus of spectroscopic observations of distant galaxies: the evolution of the star formation rate density (SFRD) in the universe has been extensively studied (e.g., Karim et al. 2011; Madau & Dickinson 2014; Khostovan et al. 2015; Abramson et al. 2016). The majority of these studies indicates that the SFRD increased from high redshift to $z \sim 2$, and has since been decreasing steeply. Coupled with this are number density evolution studies that show an increasingly dominant population of quiescent galaxies (e.g., Pozzetti et al. 2010; Brammer et al. 2011; Moustakas et al. 2013; Muzzin et al. 2013a).

Another approach is to use advanced analysis techniques to trace SFHs from photometric measurements (Pacifci et al. 2016; Iyer & Gawiser 2017); however, individual galaxy evolution is not easily traced with this method due to high uncertainties. In this case, one can investigate average SFHs of galaxies as Pacifci et al. (2016) have done by applying spectral energy distribution models to compute the median SFHs of 845 quiescent galaxies at $0.2 < z < 2.1$. They found that galaxy stellar mass is a driving factor in determining how evolved galaxies are, with high-mass galaxies being the most evolved at any time. The limitation of these approaches is that we cannot connect progenitors to descendants: studies from mass-matched samples have resulted in multiple solutions (e.g., Torrey et al. 2017). To understand the mechanics of how galaxies evolve, it is crucial to expand our view from focusing on the population of galaxies as a whole, to investigating how the star formation rate (SFR) of individual galaxies varies with time.

Probing the SFHs of individual galaxies, however, still requires high-resolution, high-quality stellar continuum spectra, which are expensive to obtain. Consequently, high-redshift samples are small and often selected with criteria to optimize data quality and sample size rather than represent the full galaxy population. Jørgensen & Chiboucas (2013) obtained spectra for ~ 80 cluster galaxies at $z = 0.5\text{--}0.9$ and found ages of 3–6 Gyr, consistent with passive evolution between $z \sim 2$ and the present. Stellar population measurements of ~ 70 $z \sim 0.7$ galaxies with stellar masses $> 10^{10} M_{\odot}$ were performed by Gallazzi et al. (2014); they found that passive galaxies have ages and metallicities consistent with those of present-day galaxies, and that star-forming galaxies require further SF and metal enrichment to evolve into present-day descendants. Choi et al. (2014) analyzed stacked spectra of thousands of passive galaxies in the redshift range $0.1 < z < 0.7$ and also found age evolution consistent with mostly passive evolution, with little dependence on mass at $z > 0.5$. Belli et al. (2015) measured ages of 1–4 Gyr for several dozen passive galaxies at redshifts $1 < z < 1.6$, indicating that we are approaching the cosmic epoch at which massive, passive galaxies stopped forming stars. Finally, at $z > 1.5$, measurements are limited to stacked spectra (e.g., Whitaker et al. 2013; Onodera et al. 2015) or sample sizes ranging from single objects to a handful (e.g., van Dokkum & Brammer 2010; Toft et al. 2012; van de Sande et al. 2013; Kriek et al. 2016). The typical age of massive, passive galaxies at those redshifts is found to be 1 Gyr or less, with short formation timescales. From this brief review, it is evident that samples at large lookback time are generally small and/or stacked. Furthermore, ages are usually estimated by assuming a single stellar population, which is arguably justified

for very massive galaxies at late cosmic epochs, but not in general.

The Large Early Galaxy Astrophysics Census (LEGA-C, van der Wel et al. 2016) survey is collecting high S/N spectra of ~ 3000 galaxies in the redshift range $0.6 < z < 1$, selected only by their K -band magnitude (a proxy for stellar mass). The data, which are comparable in quality to those obtained in the nearby universe, probe the internal kinematics of stars and gas, and the ages and metallicities of stellar populations. This enables us, for the first time, to reconstruct the SFHs of individual galaxies at large lookback time that are representative of the population. These reconstructed SFHs can provide a direct connection between progenitors and descendants, and allow us to constrain when, and how quickly, galaxies formed their stars.

Over the past decade, there have been several algorithms developed to recover SFHs, viz. *MOPED*, *STARLIGHT*, *STECMAP*, *VESPA*, *ULYSS*, and *FIREFLY* (Heavens et al. 2000; Cid Fernandes et al. 2005; Ocvirk et al. 2006; Tojeiro et al. 2007; Koleva et al. 2009; Wilkinson et al. 2015). We develop our own approach in this study to tailor the problem for galaxies at $z \sim 1$. The main differences between our algorithm and some of those listed above are the use of composite stellar populations (a group of stars that range in age within a given interval) instead of simple stellar populations (stars born from a single burst in SF); using a defined set of template spectra that allow for direct comparisons of the SFHs; as well as the assumption of constant SF within a given time interval. The galaxy spectra are also not continuum-normalized in the fitting process, but photometry is used to calibrate the fluxes.

The goal of this paper is to reconstruct the SFHs of galaxies in the LEGA-C sample and investigate the dependence of individual SFHs on stellar mass, stellar velocity dispersion, and SF activity. The paper is outlined as follows. In Section 2, we give a brief overview of the LEGA-C data set. In Section 3, we introduce the model for reconstructing the SFHs of the galaxies as well as tests of the model. In Section 4, we present a sample of the resultant fits and general trends of measured parameters. In Section 5, we investigate the SFH as a function of stellar velocity dispersion and stellar mass. We demonstrate that we can verify the relation between the evolution of SFHs and mass, and we investigate the variation in the reconstructed SFHs, at fixed stellar velocity dispersion. Finally, in Section 5, we summarize the results. A Λ CDM model is assumed with $H_0 = 67.7 \text{ km s}^{-1} \text{ Mpc}^{-1}$, $\Omega_m = 0.3$, and $\Omega_{\Lambda} = 0.7$.

2. Data

LEGA-C (van der Wel et al. 2016) is an ongoing ESO Public Spectroscopic survey with VLT/VIMOS of ~ 3000 galaxies in the COSMOS field (R.A. = $10^{\text{h}}00^{\text{m}}$, decl. = $+2^{\circ}12'$). The galaxies were selected from the Ultra-VISTA catalog (Muzzin et al. 2013b), with redshifts in the range $0.6 < z < 1.0$. The galaxies were K -band selected with a magnitude limit ranging from $K(AB) = 21.08$ at $z = 0.6$ to $K(AB) = 20.7$ at $z = 0.8$ to $K(AB) = 20.36$ at $z = 1.0$ (stellar masses $M_{*} > 10^{10} M_{\odot}$). These criteria were chosen to reduce the dependence on variations in age, SF activity, and extinction, as well as to ensure that the targets were bright enough in the observed wavelength range ($0.6\text{--}0.9 \mu\text{m}$) to obtain high-quality, high-resolution spectra ($R \sim 3000$). Each galaxy is observed for ~ 20 hr, which results in spectra with $S/N \sim 20 \text{ \AA}^{-1}$.

The analyses in this work are based on the first-year data release,¹³ which contains spectra of 892 galaxies, 678 of which are in the primary sample and have an $S/N > 5 \text{ \AA}^{-1}$ between rest-frame wavelengths 4000 and 4300 \AA (typically, $S/N \sim 20 \text{ \AA}^{-1}$). Emission line subtracted spectra are used in the fitting algorithm; therefore, the emission line spectrum of each galaxy, computed using the Penalized Pixel-Fitting method (pPXF, Cappellari & Emsellem 2004), is subtracted from the observed spectrum. For details of the emission line fitting procedure, see Bezanson et al. (2018). As part of the analysis of the model, we use the following measured quantities: stellar velocity dispersions (σ_*), 4000 \AA break (D_n4000), and $H\delta$ equivalent width indices [$EW(H\delta)$], $U - V$ colors, stellar masses ($M_{*,\text{FAST}}$), UV+IR SFRs, and UV+IR specific SFRs ($s\text{SFR}_{\text{UV+IR}}$). Stellar masses are determined using FAST (Kriek et al. 2009) based on photometric measurements, Bruzual & Charlot (2003) stellar population libraries, adopting a Chabrier (2003) Initial Mass Function (IMF), Calzetti et al. (2000) dust extinction, and exponentially declining SFRs. The UV+IR SFRs are estimated from the UV and IR luminosities, following Whitaker et al. (2012). For details of the data reduction procedure, see van der Wel et al. (2016).

3. Spectral Fitting Technique

3.1. Stellar Population Model

To reconstruct the SFHs of galaxies, one needs to gauge the various ages of stellar populations within these galaxies. This is done using stellar population spectra (SSPs) generated with the Python implementation of the Flexible Stellar Population Synthesis package (*FSPS* v3.0; Conroy et al. 2009; Conroy & Gunn 2010; Foreman-Mackey et al. 2014), using the MILES spectral library (Sánchez-Blázquez et al. 2006), Padova isochrones (Girardi et al. 2000; Marigo & Girardi 2007; Marigo et al. 2008) and a Kroupa IMF (Kroupa et al. 2001).

A galaxy spectrum is approximated to be a linear combination of template spectra at varying ages, attenuated by dust:

$$f_\lambda = \sum_{i=1}^n m_i T_{\lambda,i} 10^{-0.4k_\lambda E(B-V)_i}, \quad (1)$$

$$k_\lambda = 2.659 \left(-2.156 + \frac{1.509}{\lambda} - \frac{0.198}{\lambda^2} + \frac{0.011}{\lambda^3} \right) + 4.05,$$

where n is the number of SSP to fit to the galaxy, $T_{\lambda,i}$ are the template spectra, m_i are the weights that scale the templates to match the spectra of the galaxy, k_λ is the reddening curve (Calzetti et al. 2000), and $E(B - V)_i$ are the dust reddening values.

We generate 12 composite stellar population spectra (CSPs), with solar metallicity (see Section 3.3), covering ages from 0 to about 7 Gyr, the age of the universe in LEGA-C's redshift range. To determine the intervals of the 12 age bins of the CSPs, simple SSPs were generated and the cumulative absolute difference from one spectrum to another was calculated as the age was increased; which was then divided into 12 percentiles with equal width (see Table 1 and Figure 1 for the properties of the CSPs in each age bin). This method of determining the time intervals generates template spectra that optimize the temporal

Table 1
Properties of the FSPS Template Spectra

Age Bin ^a log(year)	SFR ^b $M_\odot \text{ yr}^{-1}$	M_* ^c M_\odot	$L_{\text{bol}*}$ ^d $\log(L_\odot)$
0.000–8.000	1.000×10^{-8}	0.837	1.964
8.000–8.300	1.005×10^{-8}	0.711	0.885
8.300–8.475	1.010×10^{-8}	0.748	0.650
8.475–8.650	6.750×10^{-9}	0.731	0.497
8.650–8.750	8.646×10^{-9}	0.718	0.382
8.750–8.875	5.332×10^{-9}	0.707	0.285
8.875–9.000	3.998×10^{-9}	0.695	0.187
9.000–9.075	5.305×10^{-9}	0.685	0.127
9.075–9.225	2.040×10^{-9}	0.671	0.099
9.225–9.375	1.444×10^{-9}	0.652	−0.043
9.375–9.525	1.022×10^{-9}	0.639	−0.161
9.525–9.845	2.681×10^{-10}	0.618	−0.347

Notes.

^a Age interval of CSP templates.

^b SFR s.t. $1 M_\odot$ of stars formed within the interval.

^c Stellar mass (including stellar remnants) with mass loss accounted for.

^d Bolometric luminosity.

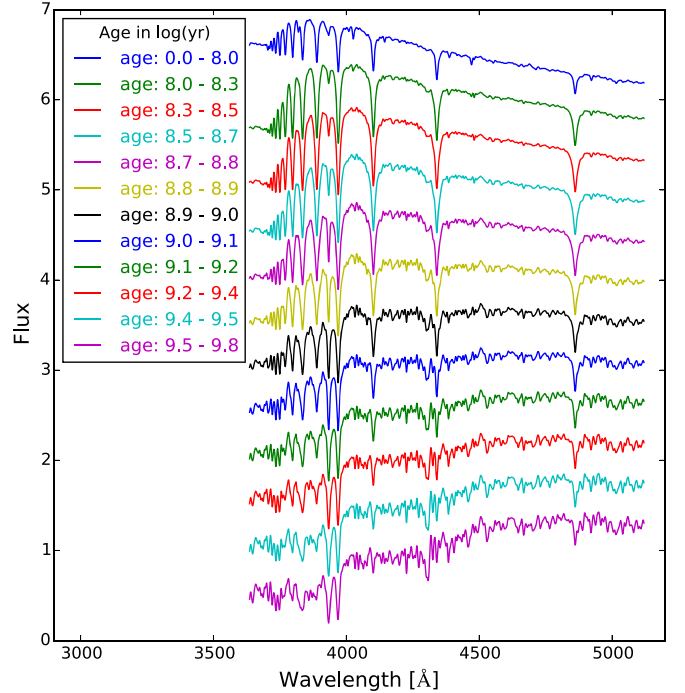


Figure 1. Template CSP spectra used to fit LEGA-C galaxies. They were generated from FSPS, using the time intervals listed in Table 1, with solar metallicity and arbitrary velocity dispersion; and they have been normalized and shifted here for comparison purposes.

sampling of an evolving stellar population. In practice, the age bins are ~ 0.15 dex wide over the age range 0–7 Gyr.

The template spectra are generated with a constant SFR and are normalized such that $1 M_\odot$ of stars are formed within each time bin (stellar masses include stellar remnants). Note that there is mass loss in each bin as massive stars die off (see Table 1). We assume a constant SFR within each time bin as it presents a more realistic evolution of a galaxy's SF with time, and can take into account rapid changes in the SFH. Choosing SSP templates would not lead to significantly different SFHs; however, it would lead to aliasing effects when reconstructing

¹³ <http://www.eso.org/qi/catalogQuery/index/93>

the SFHs for samples of galaxies. The templates are also broadened to the velocity dispersion of the galaxies (Bezanson et al. 2018). It is assumed that dust reddening is the same for all populations except for the youngest population (age < 100 Myr). Dust extinction is expected to be different for young stellar populations as they are usually observed to be nested in the dust of their molecular birth clouds (Charlot & Fall 2000). Therefore, two dust reddening values are fit: $E(B - V)_1$, for the age range 0–100 Myr, and $E(B - V)_2$, for the rest of the age ranges.

3.2. Fitting Algorithm

To find the optimal values for the 14 parameters, viz. the 12 weight factors (m_i) for the 12 CSP templates and 2 dust reddening values ($E(B - V)_i$), we used *emcee*, a Python implementation of an affine invariant ensemble sampler for MCMC (Foreman-Mackey et al. 2013), which was proposed by Goodman & Weare (2010). It uses MCMC “walkers,” which randomly explore the parameter space, where each proposed step for a given walker depends on the positions of all the other walkers in the ensemble, with the aim of converging to the most likely parameter values.

The priors for the 14 parameters were set such that all parameter values were always greater or equal to 0, and the upper limit for $E(B - V)_i$ was set to 3. The parameter value for the youngest bin was initially set to be equal to the measured SFR from UV+IR measurements, but it was allowed to vary between 1/3 and 3 times that value during the fitting process, allowing for measurement errors. For the other bins, the best-fitting single template, computed using least-squares fitting, was assigned all the stellar mass, with all other parameter values set to 10^{-6} . Starting with equal SFRs in all bins also recovers the SFHs, however, the algorithm may take longer to converge to the optimal values.

For each galaxy, 100 MCMC walkers were used, initiated in a small region around the starting values mentioned above. A total of 20,000 samples were taken and 1000 steps were kept after burn-in. The mean acceptance fraction was $\gtrsim 0.2$ and the typical autocorrelation time was ~ 95 iterations. The optimal values for the parameters are taken as the 50th percentile of the list of samples of the converged walkers, and the lower and upper uncertainties are the 16th and 84th percentiles, respectively. The fitting algorithm resulted in 607 good fits based on their normalized χ^2 values (< 5 , from visual inspection of the fits), and these were used in the analyses. The spectra that were not well fit were mainly due to low S/N and AGN.

3.3. Robustness of Fitting Results

To assess the robustness of the model, we performed the following tests: generate and fit synthetic spectra; compare model stellar mass measurements of the LEGA-C population with those obtained from broadband photometry (see Section 2); fit a sample of SDSS spectra and compare model stellar masses with literature measurements; and test the assumption of solar metallicity.

Synthetic galaxy spectra were generated with varying SFHs using the CSPs in Section 3.1, including simulated noise that mimics LEGA-C variance spectra, to compare how well the algorithm recovered the SFHs. Twenty SFHs were generated for each S/N (5, 10, 20, 30, 40, 50, and 60 \AA^{-1}), and the

average deviations of the true a_{MW} , stellar mass, and luminosity from the best-fitting model parameters were computed. In general, the model sufficiently recovered the SFHs; however, we note that the quality of the results depends on the noise introduced into a spectrum (see Figure 2 for two examples). Stellar mass and luminosity are recovered with precision ≤ 0.1 dex for $S/N \geq 20$, while a_{MW} only requires $S/N \geq 10$ to reach the same level of precision. We note that these tests only constrain the purely random uncertainties due to the noise in the spectra, while they do not include systematic errors in the data (e.g., sky subtraction, flux calibration) and systematic uncertainties in the FSPS model spectra.

Imposing the MCMC model on the LEGA-C data set and comparing the stellar masses measured from the model to those measured from FAST (using photometric measurements), resulted in very good agreement between the two methods, with a scatter of ~ 0.2 dex and an offset of ~ 0.03 dex. This scatter is larger than the formal uncertainty on our mass measurements (~ 0.15 dex).

We used the fitting algorithm on a sample of 20 SDSS spectra of massive local galaxies ($z \sim 0.1$), selected by stellar mass ($M_* > 10^{10}$), to determine whether the model could recover the stellar masses measured in the literature. We compared the model stellar masses to measurements from the Portsmouth method (Maraston et al. 2009) and found satisfactory agreement, with a ~ 0.2 dex scatter. The maximum age of the templates was increased to ~ 12 Gyr to account for the low redshift (~ 0.1) of the SDSS galaxies. The 0.2 dex random uncertainty is an indication of how results vary as a consequence of using a different SPS model (here, Maraston et al. 2009 versus *FSPS*) and fitting algorithm.

Solar metallicity was used to generate all the CSPs because according to Gallazzi et al. (2005, 2014), the metallicity–mass relation flattens out to solar metallicity in LEGA-C’s mass range ($\log(M) \gtrsim 10.5$), for $z \sim 0.7$ galaxies. On the other hand, Jørgensen et al. (2017) find evidence of evolution in the metallicity for cluster galaxies, as well as a trend of increasing metallicity with increasing velocity dispersion. We test our approach by repeating our fits with implausibly low metallicity ($0.4 Z_{\odot}$, subsolar) and high metallicity ($2.5 Z_{\odot}$, super-solar) CSPs. We find no significant differences in the χ^2 values of the fits, but, naturally, the inferred ages depend on the chosen metallicity. If we assign subsolar metallicity for galaxies in our sample, the derived mass-weighted and light-weighted ages are older by 0.05 and 0.08 dex, respectively, with a standard deviation of 0.16 and 0.24 dex, respectively. If we assign super-solar metallicity for the sample, the light-weighted ages are younger by 0.03 dex, with a standard deviation of 0.20 dex. The mass-weighted age changes from solar to high metallicity are not normally distributed: 80% of the galaxies have the same age to within 0.20 dex, while for the remaining 20% the change in age ranges from 0.2 to 0.9 dex. However, only 10 of these galaxies’ mass-weighted ages change by ≥ 0.5 dex and they have a mean light-weighted age of ~ 0.4 Gyr. The age changes do not depend on the measured stellar mass or stellar velocity dispersion.

The velocity dispersion–metallicity trend presented by Jørgensen et al. (2017) implies that our assumption of solar metallicity for all galaxies may introduce a correlation between velocity dispersion and age. Our tests show that across the velocity dispersion range $\sigma_* = 100\text{--}250 \text{ km s}^{-1}$, the magnitude of this effect would be at most 0.15 dex and likely less. This

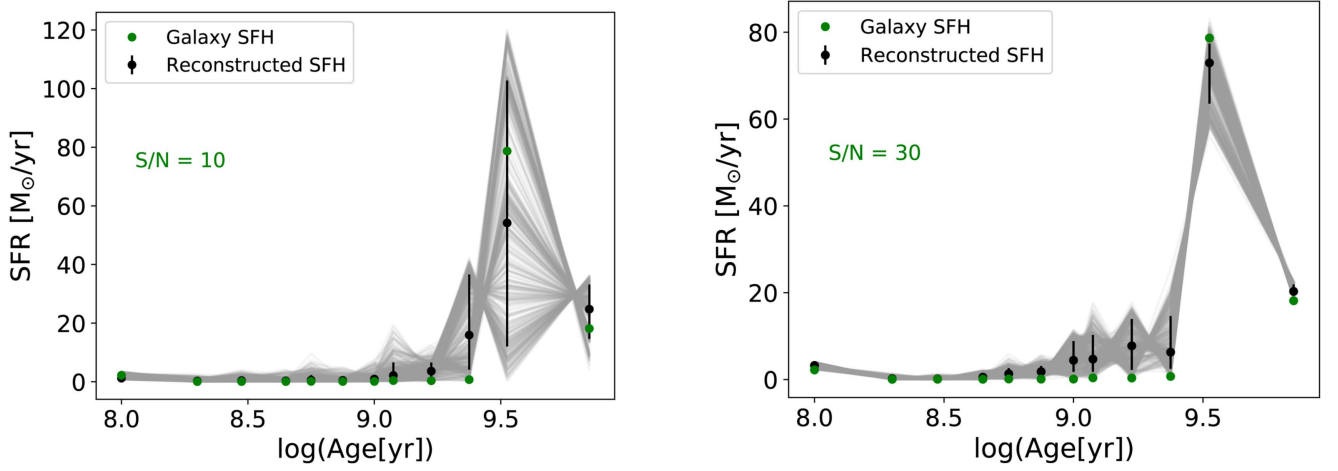


Figure 2. Reconstructed SFH (black) of a synthetic galaxy (green) with $S/N = 10 \text{ \AA}^{-1}$ (left) and $S/N = 30 \text{ \AA}^{-1}$ (right). The converged walkers are shown in gray and the upper and lower uncertainties are based on the 16th and 84th percentiles, respectively, as explained in Section 3.2. By $S/N = 30 \text{ \AA}^{-1}$, the recovered SFHs predict the stellar mass, age, and luminosity with precision ≤ 0.1 dex.

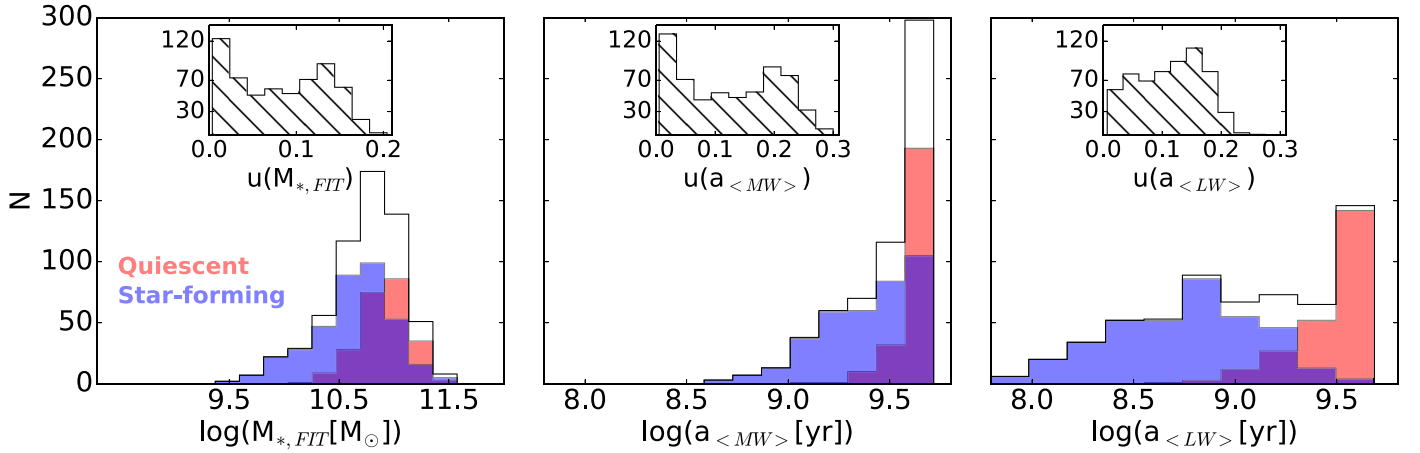


Figure 3. Distributions of $M_{*,FIT}$ (left), $a_{\langle MW \rangle}$ (middle), and $a_{\langle LW \rangle}$ (right) of the LEGA-C sample. The quiescent and star-forming populations (as defined in Section 5.1) are shown in red and blue, respectively. The distribution of the uncertainties for each parameter are shown at the top of each figure.

potential bias is insufficient to explain the σ_* -age relation we find in Section 4.2. Follow-up studies that explore the interdependence of age, metallicity, and other galaxy properties will need to take metallicity variations into account.

4. Fitting Results

4.1. Model Outputs

Figure 3 shows the distribution of the model-measured stellar masses ($M_{*,FIT}$, left panel), mean mass-weighted ages¹⁴ ($a_{\langle MW \rangle}$, middle panel) and mean light-weighted ages¹⁴ ($a_{\langle LW \rangle}$, right panel) of the LEGA-C sample, along with the distribution of uncertainties for each parameter. The distributions are separated into the quiescent (red) and star-forming (blue) populations to show the differences in the distributions based on current SF activity (see Section 5). The galaxies in the LEGA-C sample span a broad range of ages: $a_{\langle LW \rangle}$ can be as young as 60 Myr and as old as 4.8 Gyr, and has a median value of 1.2 Gyr (see Figure 3). $a_{\langle MW \rangle}$ ranges from about 400 Myr to about 5.2 Gyr, with a median value of 3.8 Gyr. However, most of these galaxies are old, with about 60% being older than

3 Gyr. The $M_{*,FIT}$ of the galaxies ranges from $\sim 2 \times 10^9 M_\odot$ to $\sim 4 \times 10^{11} M_\odot$, with a median value of about $6 \times 10^{10} M_\odot$. The formal age and mass uncertainties lie in the ranges 1%–60% and 1%–40%, respectively. As stated in Section 3.3, these uncertainties do not include systematic errors.

4.2. Sample SFHs

Figure 4 shows the spectra of a sample of LEGA-C galaxies (in $a_{\langle MW \rangle}$ order) along with the best-fitting model spectra as described by Equation (1) using the optimal parameter values from *emcee*. The weight factors, m_i , represent the SFHs of these galaxies (shown on the bottom right of each figure). The resultant normalized χ^2 , dust reddening values ($E(B - V)_i$), stellar masses ($M_{*,FIT}$), luminosities (L_{FIT}) and mean mass-weighted ages ($a_{\langle MW \rangle}$) from the model are shown in red. The sample was selected to display the wide range of SFHs recovered.

The reconstructed SFHs reveal that although most galaxies at $z \sim 1$ have $a_{\langle MW \rangle} > 3$ Gyr, the sample spans a wide range of histories. For the older massive galaxies, the oldest template (stars in the age range of ~ 3 –7 Gyr) contributes to the majority of their mass. Some of these galaxies only contain the oldest stars and have since been quiescent, i.e., for the past ~ 3 Gyr

¹⁴ Mean mass-weighted and light-weighted ages are obtained by averaging the midpoint ages of the CSPs weighted by luminosity and mass, respectively.

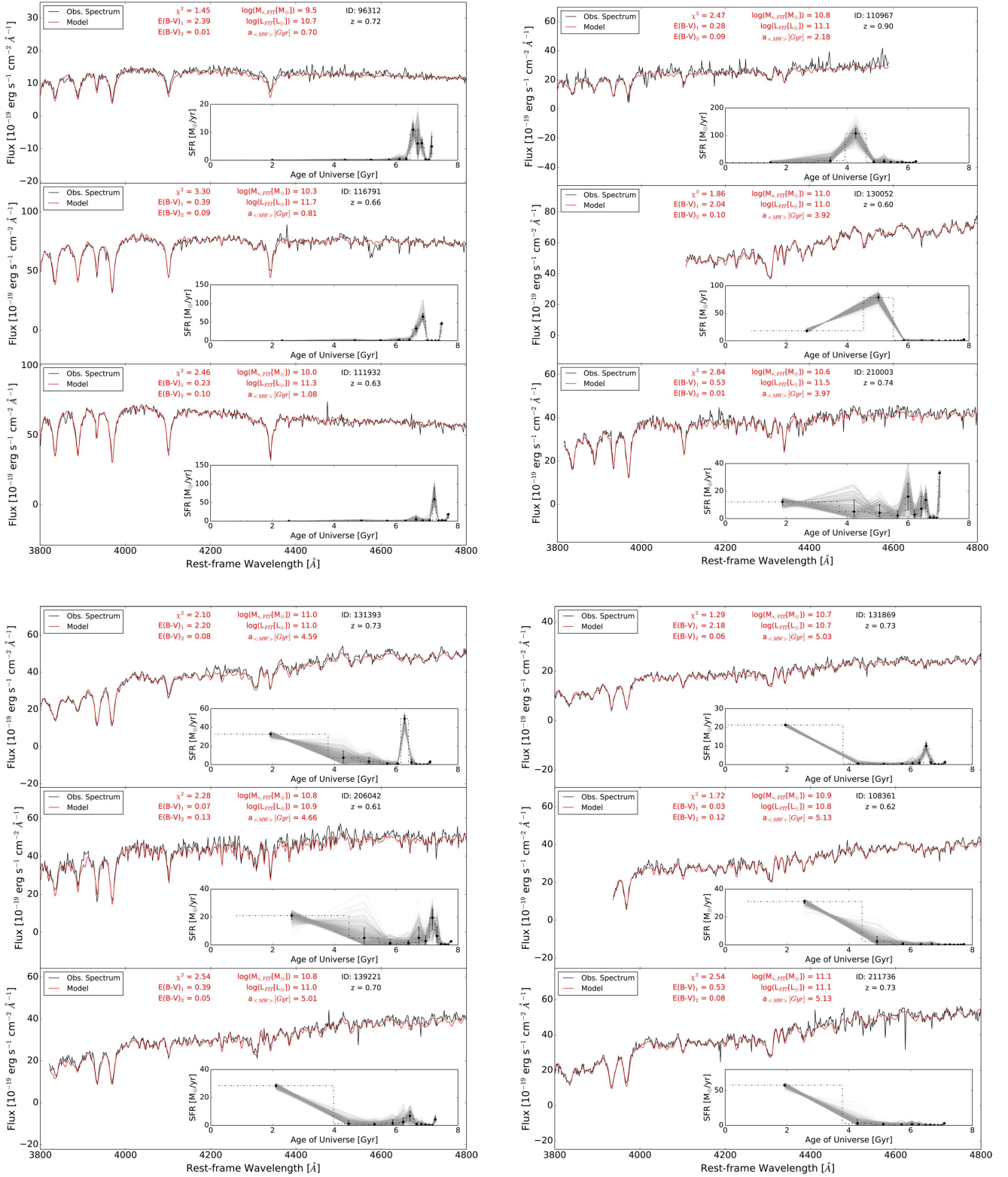


Figure 4. Sample of emission line subtracted spectra of 12 LEGA-C galaxies with the best-fitting model obtained from combining the 12 template spectra using MCMC. The bottom right figure in each plot is the reconstructed star formation history (the converged walkers are shown in gray). The MCMC resultant mass, luminosity, mass-weighted age, and dust reddening values are shown in red. The spectra are ordered by a_{MW} .

(see the SFHs of 108361, 211736, and 130052 in Figure 4). However, some galaxies were quiescent for several gigayears and then had a renewed period of growth, either due to SF rejuvenation, or merging with a younger population. A merger could result in either an integration of the younger population

with no further activity, or trigger bursts of SF. This young population of stars accounts for $\sim 10\%$ of the mass of these galaxies (e.g., 206042, 131869, and 131393 in Figure 4). We will explore the frequency of such rejuvenation events in more detail in a follow-up study.

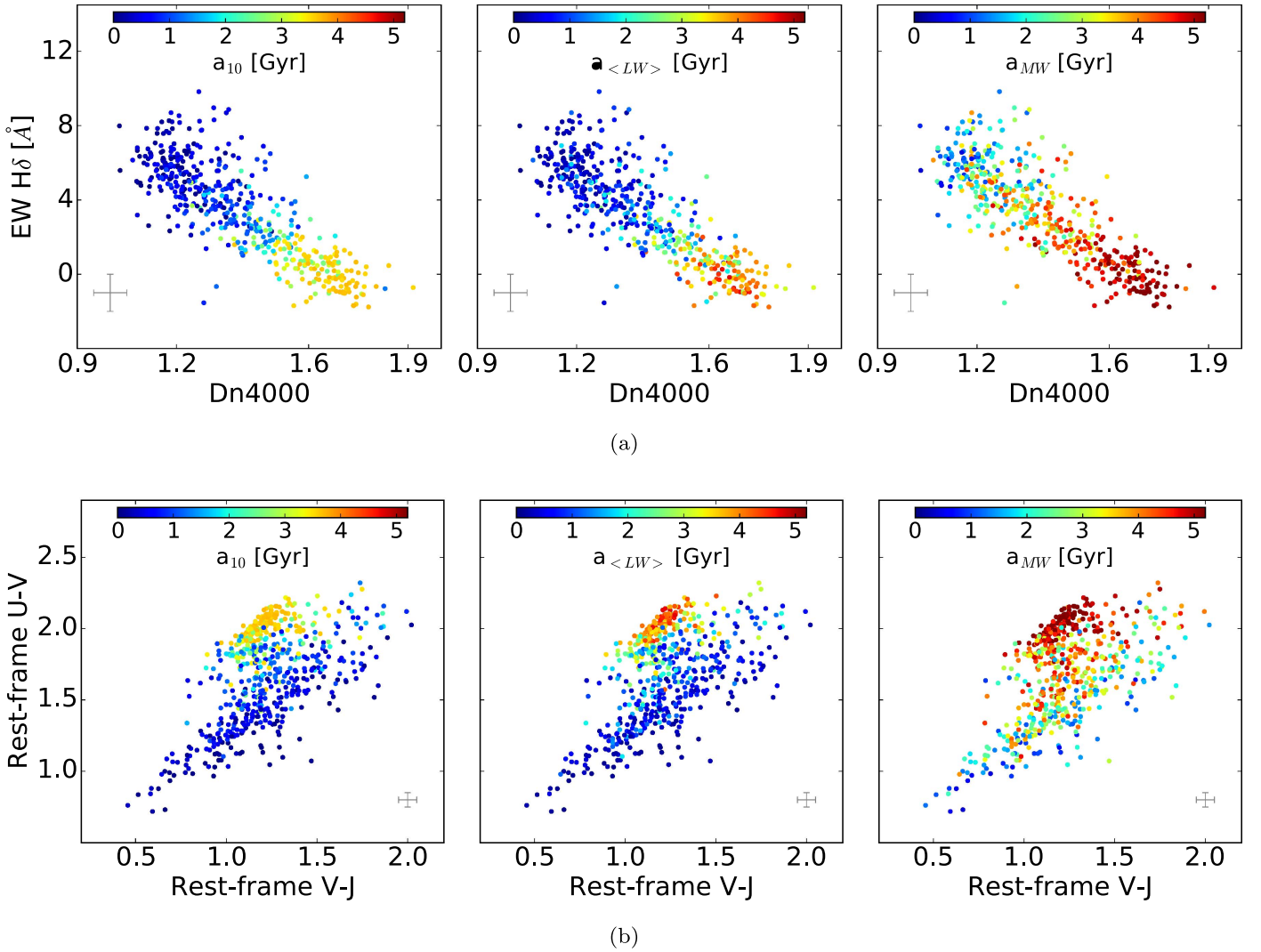


Figure 5. EW(H δ) vs. D n 4000 (upper panel) and $U - V$ color vs. $V - J$ color (lower panel) color-coded by the time after which the final 10% of stars were formed (left), the mean light-weighted age (middle), and the mean mass-weighted age (right). Typical error bars are indicated in gray.

4.3. General Trends

Figure 5(a) presents the distribution of EW(H δ) as a function of the D n 4000 break color-coded by the time after which the final 10% of stars were formed (a_{10} , left panel), $a_{\langle LW \rangle}$ (middle panel), and $a_{\langle MW \rangle}$ (right panel), estimated from the model. The EW(H δ)–D n 4000 distribution is analyzed in depth in Wu et al. (2018). As expected, for all three age parameters, galaxies generally evolve from the upper left region (high EW(H δ) and low D n 4000) to the lower right region (low EW(H δ) and high D n 4000) as they age. a_{10} and $a_{\langle LW \rangle}$ are more correlated with each other than $a_{\langle MW \rangle}$ because they track young stars; they also have smoother transitions in the EW(H δ)–D n 4000 plane because those features primarily track recent SF activity ($\lesssim 1$ Gyr). Figure 5(b) shows the rest-frame $U - V$ color as a function of rest-frame $V - J$ color-coded by the same three age parameters as above. Once again, expected trends are seen: a_{10} , $a_{\langle LW \rangle}$, and $a_{\langle MW \rangle}$ correlate with the rest-frame colors as $U - V$ and $V - J$ primarily reflect recent SF (~ 1 Gyr). There is a notable population of old galaxies ($a_{\langle MW \rangle} > 3.5$ Gyr) with relatively blue colors, which indicates that these galaxies have extended SFHs.

To demonstrate the validity of the old galaxies ($a_{\langle MW \rangle} > 3.5$ Gyr) in the young region of the EW(H δ)–D n 4000 plane, i.e., galaxies in red in Figure 5’s right panel, with D n 4000 < 1.3 and EW(H δ) > 2 , we refer to their SFHs. These galaxies formed most of their stars early on, but also have significant recent SF. While some seem to have been quiescent at some point in their history before they were possibly rejuvenated or merged with another galaxy (e.g., 206042 in Figure 4), others formed stars throughout their history (e.g., 210003 in Figure 4). Moreover, the presence of young and old populations can be seen in their spectra: they have clearly visible Balmer lines, characteristic of younger galaxies; but they also have H and K absorption lines of singly ionized calcium with similar strengths, which is typical of older galaxies, in addition to the presence of the G -band (absorption lines of the CH molecule) around 4300 Å. As a test, we reran the fits of these galaxies excluding the three oldest templates and found that the spectra cannot be well fit.

There is also a population of galaxies that seems to contain only young stars (e.g., 111932 and 116791 in Figure 4), which would imply that these galaxies formed more than 90% of their

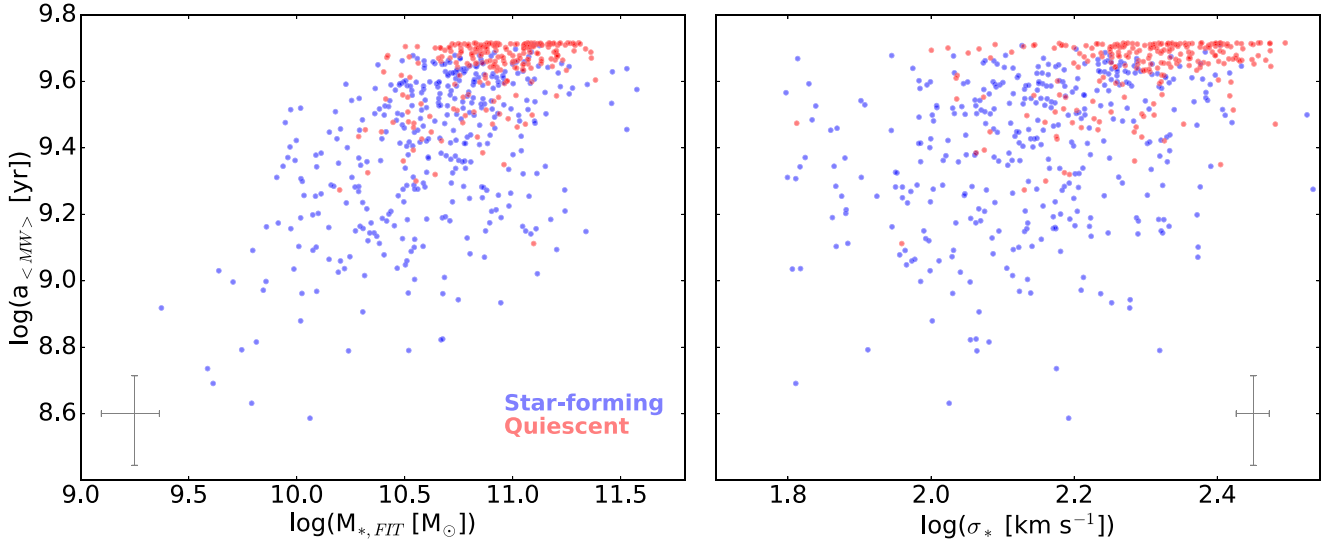


Figure 6. $a_{\langle MW \rangle}$ as a function of $M_{*,FIT}$ (left) and σ_* (right). The star-forming and quiescent populations are indicated in blue and red, respectively, and typical error bars are indicated in gray. Galaxies with $\sigma_* \gtrsim 200 \text{ km s}^{-1}$ are almost exclusively old ($>4 \text{ Gyr}$) and quiescent, which indicates that σ_* is a stronger predictor of age and SF activity.

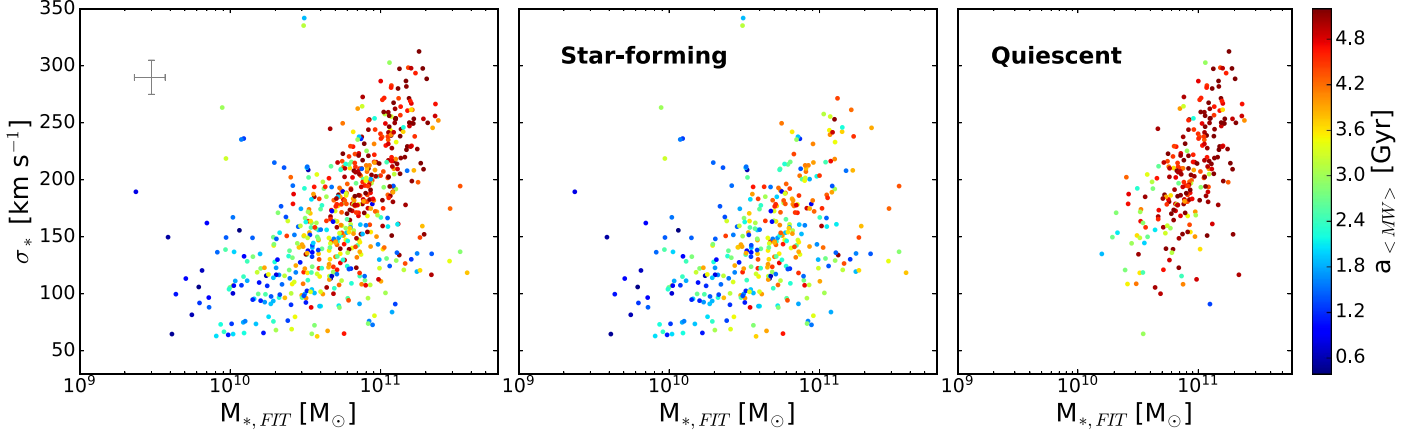


Figure 7. σ_* vs. $M_{*,FIT}$, color-coded by $a_{\langle MW \rangle}$. The star-forming and quiescent populations are shown in the middle and right panels, respectively. Typical error bars are indicated in gray. The clear separation between young and old galaxies at $\sigma_* \sim 170 \text{ km s}^{-1}$ shows a stronger correlation between $a_{\langle MW \rangle}$ and σ_* over $M_{*,FIT}$, which also depends on the current SF activity.

mass recently (when the universe was $>6 \text{ Gyr}$). To test if young populations are “outshining” the rest of these galaxies, i.e., if there are hidden populations of old stars, we reran the fits of these galaxies allowing only the oldest template parameter to vary. We found that the contribution in mass of the old population can increase by $\sim 5\%–10\%$ before the normalized χ^2 changes by more than 0.08 dex. The change in χ^2 is mainly due to the continuum shape of the spectra. Therefore, these galaxies do not harbor significant populations of old stars that are concealed by the light of very young stars.

5. SFHs of the Galaxy Population

5.1. Correlations between Age, $M_{*,FIT}$, and σ_*

Figure 6 shows $a_{\langle MW \rangle}$ as a function of stellar mass ($M_{*,FIT}$, left panel) and stellar velocity dispersion (σ_* , right panel) color-coded by current SF activity, i.e., whether the galaxy is quiescent ($\log(\text{sSFR}_{UV+IR}[\text{Gyr}^{-1}]) < -1$) or star-forming. Selecting quiescent galaxies by their $U - V$ and $V - J$ colors would result in similar trends. $a_{\langle MW \rangle}$ generally correlates more strongly with $M_{*,FIT}$ than σ_* . However, there is a σ_* threshold

above which galaxies are almost exclusively old and quiescent: galaxies with $\sigma_* > 200–250 \text{ km s}^{-1}$ and $a_{\langle MW \rangle} < 4 \text{ Gyr}$ are very rare. Such a clear threshold does not exist for $M_{*,FIT}$: high-mass galaxies ($M_{*,FIT} \gtrsim 10^{11} M_{\odot}$) show a variety of ages.

To further illustrate these trends, we show σ_* as a function of $M_{*,FIT}$ color-coded by $a_{\langle MW \rangle}$ (left panel) and divided by current SF activity (middle and right panels) in Figure 7. There is a discernible separation between old ($>4 \text{ Gyr}$) and young ($<4 \text{ Gyr}$) galaxies at a velocity dispersion of $\sigma_* \sim 170 \text{ km s}^{-1}$. Taken together with the trends seen in Figure 6, we can conclude that $\sigma_* > 250 \text{ km s}^{-1}$ is a sufficient requirement for having an old age and $\sigma_* \sim 170 \text{ km s}^{-1}$ is a necessary requirement for old age. This extends the properties of present-day early-type galaxies, for which a correlation between velocity dispersion (and closely related quantities such as surface mass density and central mass density) and stellar age has been shown to be more fundamental than age trends with stellar mass (Kauffmann et al. 2003; Graves et al. 2009; van der Wel et al. 2009), to higher redshift. Our results also extend the widely reported correlation between velocity dispersion (as well as surface mass density and central mass density) and SF activity (e.g., Franx et al. 2008; Barro et al.

2017; Mosleh et al. 2017) to an underlying correlation with overall stellar age.

The scaling relation between σ_* and black hole (BH) mass implies that large BH mass is correlated with early SF and the ceasing thereof. Such a scenario is supported by the direct correlation between BH mass and SF activity (e.g., Terrazas et al. 2016) and the large fraction of radio AGNs among galaxies with large velocity dispersions both at low and high redshifts (e.g., Best et al. 2005; Barišić et al. 2017).

It is interesting to note that the correlation between $a_{(\text{MW})}$ and σ_* seen in Figure 7 is significantly weakened after dividing the population by current SF activity. Instead, for the star-forming population, galaxy age is better correlated with $M_{*,\text{FIT}}$ (also seen in Figure 6). A straightforward interpretation is that when galaxies are growing rapidly through SF—that is, when they are located on or near the SF “Main Sequence”—then M_* mostly traces how long this main SF phase has lasted so far. In other words, M_* simply traces the build-up of the stellar population over time, while σ_* is related to the end of this main SF phase, i.e., to the regulation and cessation of SF, presumably through AGN feedback.

5.2. Evolution of the Average SFHs

The average SFHs of galaxies, normalized by stellar mass, as a function of σ_* and $M_{*,\text{FIT}}$ are shown in Figures 8(a) and (b), respectively. The average SFHs were corrected for completeness by weighing each galaxy by a completeness correction factor to create a volume-limited quantity (see Wu et al. 2018). The population is divided by its current SF activity in order to disentangle the effects from these two populations as well as to compare them. The velocity dispersion and mass ranges were selected such that there were enough galaxies in each bin (≥ 10), in both quiescent and star-forming galaxies. These relations are used to determine whether $z \sim 1$ galaxies also show a downsizing trend in their SFHs, as many studies have pointed to using local galaxies. However, the SFHs seen at $z \sim 1$ would not be resolved at $z \sim 0.1$, as the stellar populations would be too old.

On average, high- σ_* galaxies ($\sigma_* \geq 170 \text{ km s}^{-1}$) had higher SFRs at earlier epochs that started to decline rapidly, at a rate that increases with σ_* and stellar mass, when the universe was ~ 3 Gyr old. Most galaxies with lower velocity dispersions ($\sigma_* < 170 \text{ km s}^{-1}$) gradually build their stellar mass as the universe evolves; however, the SFR of a minority, i.e., the quiescent population, began to decline when the universe was ~ 5 Gyr old. Higher-mass star-forming galaxies ($M_{*,\text{FIT}} \geq 10^{10.5} M_\odot$) have SFHs that are consistent with constant SF with time, while the lower mass galaxies ($M_{*,\text{FIT}} < 10^{10.5}$) still have rising SFRs. The star-forming population is still undergoing its main formation phase. The SFH trend is clear with $M_{*,\text{FIT}}$ and not σ_* for the star-forming population, which extends from $M_{*,\text{FIT}}$ being better correlated with SFHs for star-forming galaxies as discussed in Section 5.1 (see Figures 6 and 7).

Figure 8 reveals that, on average, most galaxies in the sample were forming stars quite early on; however, the SFRs were systematically higher and the eventual decline systematically more rapid with increasing σ_* ($M_{*,\text{FIT}}$ for the star-forming population). This is clear evidence for the top-down scenario; where galaxies downsize in their SF with time (more massive galaxies have older stars). This is seen in the overall population, and more strongly so in the quiescent population. While this result is in alignment with previous studies for the

local universe (e.g., Juneau et al. 2005; Thomas et al. 2005; Tojeiro et al. 2009; McDermid et al. 2015; Ibarra-Medel et al. 2016), our work establishes this trend at $z \sim 1$ (half the current age of the universe) using full spectrum fitting. Wu et al.’s (2018) study of the D_n4000 and H δ spectral features also supports the downsizing scenario.

5.3. The Variety of SFHs

In Figure 9, we show all the stellar mass normalized SFHs in the LEGA-C sample, separated into four velocity dispersion bins and divided into the quiescent and star-forming population (at the observed redshift) as defined in Section 5.1. This reveals the large scatter in the SFHs at fixed mass, in addition to discerning the differences in the histories based on the current SF activity of the galaxies.

The SFHs of quiescent galaxies peaked early on in the universe and thereafter, their activity generally decreases with time; while star-forming galaxies gradually grow in SFR, which peaked at later epochs. The quiescent population has consistently higher SFRs at early epochs, whereas its star-forming counterpart has higher SFRs at later epochs. This indicates that star-forming galaxies aggregate their mass slower than the quiescent population. The dominance of the quiescent population increases from low- to high-mass galaxies, and vice versa for the star-forming population.

The SFRs of low-mass galaxies ($\sigma_* < 115 \text{ km s}^{-1}$) have been gradually increasing, with large scatter at all epochs. These galaxies are currently undergoing the main stages of their SF. Note that the lowest dispersion bin suffers from incompleteness, due to the survey sample selection approach. *K*-band quiescent galaxies are fainter than equally massive star-forming galaxies, which causes an under-representation in the LEGA-C sample. However, it is well known that low-mass star-forming galaxies outnumber quiescent galaxies of the same mass; therefore, the SFHs in Figure 9 can be considered illustrative.

The quiescent and star-forming populations are more evenly distributed (in number and variation of SFHs) in the intermediate- σ_* regime (between 160 and 205 km s^{-1}), while the high- σ_* population ($\sigma_* \geq 205 \text{ km s}^{-1}$) is dominated by quiescent galaxies. The disparity between the SFHs of the quiescent and star-forming populations in the high- σ_* regime indicates that galaxies “remember” their past. There is a strong coherence among the SFHs of quiescent and star-forming galaxies, respectively. This behavior extends to the peak of cosmic SF activity at $z \sim 2-3$. This implies that SF activity at the moment of observation is strongly correlated with the SF activity ~ 3 Gyr prior. The results of this work indicate that many evolutionary paths can lead to galaxies at a given velocity dispersion. This illustrates the difficulty of connecting progenitor and descendant populations at different cosmic epochs.

5.4. Comparisons to Literature Measurements

As stated in Section 5.2, the deconstructed SFHs in this study support the galaxy downsizing scenario, which has long been studied (see Section 1). Leitner’s (2012) finding that star-forming galaxies formed only $\sim 15\%$ of their mass before $z = 1-2$ (mass dependent), suggesting that present-day star-forming galaxies are not the descendants of massive star-forming galaxies at $z > 2$, is in line with our results since the

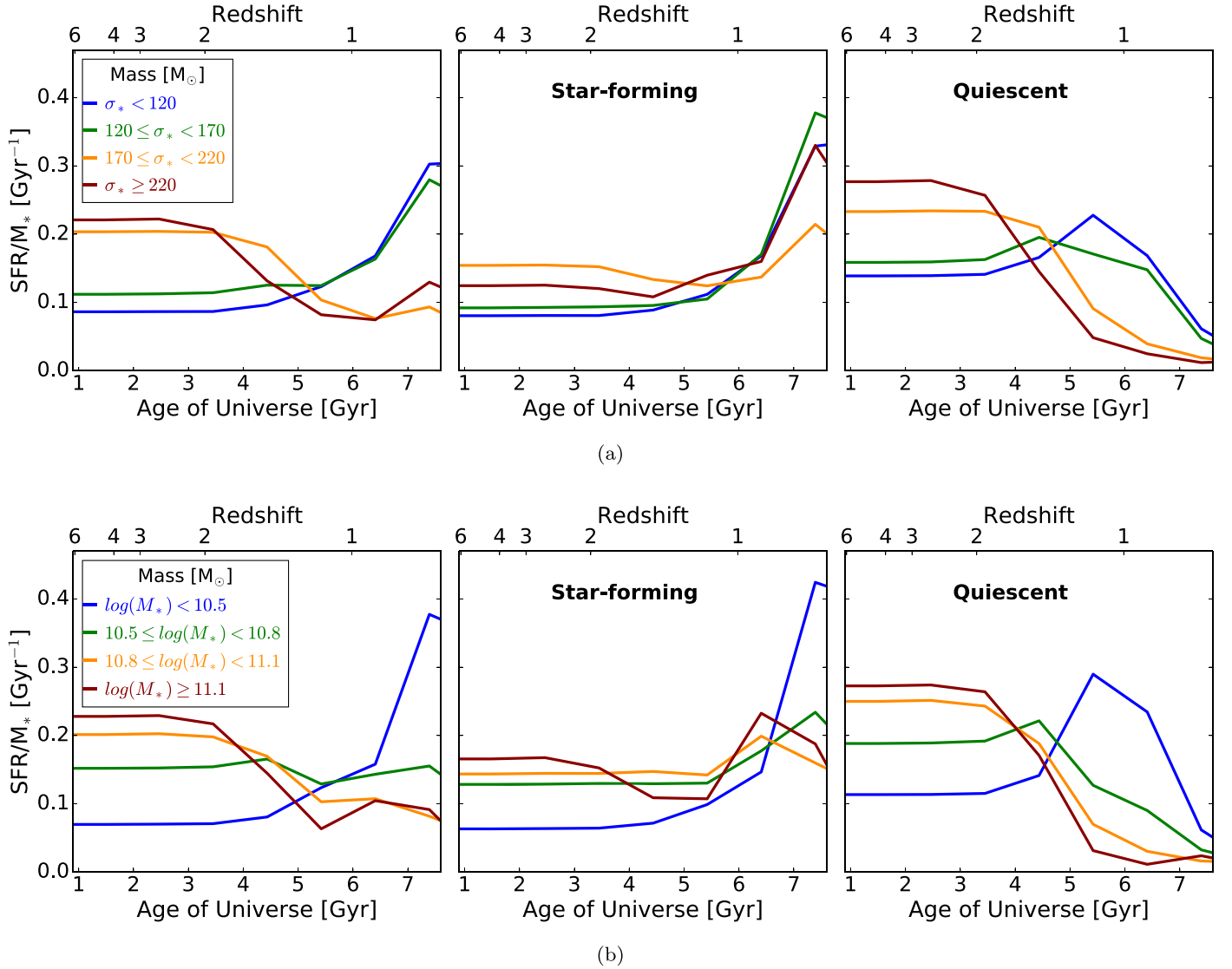


Figure 8. Ensemble-averaged SFHs of LEGA-C galaxies, normalized by stellar mass and separated into various σ_* (top) and $M_{*,\text{FIT}}$ (bottom) bins. The histories are divided into the star-forming and quiescent populations in the middle and right panels, respectively. The stellar content in massive galaxies formed earlier and faster, regardless of current SF activity.

peak in SF occurs after $z < 1.5$ for almost all star-forming galaxies in the LEGA-C sample.

Intermediate-redshift stellar population studies are sparse, due to the high S/N required to undertake such studies (see Section 1). Pertaining to this work, there are a few studies we can draw comparisons from, viz. Choi et al. (2014) and Gallazzi et al. (2014). Measurements by Choi et al. (2014) and Gallazzi et al. (2014) indicating that passive galaxies have ages consistent with mostly passive evolution are also in alignment with this study, as the reconstructed SFHs indicate that galaxies stay quiescent, barring some histories that showed low-level SF after quiescence. Gallazzi et al. (2014) reported an average lighted-weighted age of ~ 5 Gyr for a $4 \times 10^{10} M_\odot$ galaxy, consistent with our value of 4.8 Gyr, for a galaxy of the same mass.

Diemer et al. (2017) tested Gladders et al.’s (2013) hypothesis that the SFHs of individual galaxies are characterized by a log-normal function in time, which implies a slow decline in SFRs rather than rapid quenching. They did this by

comparing the log-normal parameter space of total stellar mass, peak time, and full width at half maximum of simulated galaxies from Illustris (Vogelsberger et al. 2014) and Gladders et al. (2013), as well as Pacifici et al.’s (2016) derived SFHs of a sample of quiescent galaxies using a large library of computed theoretical SFHs. They found good agreement for all three studies; however, Illustris predicted more extended SFHs on average. LEGA-C galaxies support the slow-quenching picture of galaxy evolution as Gladders et al. (2013) have suggested, with a rate of decline that is mass dependent as we have seen. More comparisons will be performed in later papers.

6. Summary

We have reconstructed the SFHs of galaxies in the current LEGA-C sample, which contains 678 primary sample galaxies with $S/N \sim 20 \text{ \AA}^{-1}$ in the redshift range of $0.6 < z < 1$. We have done this by implementing an algorithm to fit flexible SFHs to the full spectrum, using FSPS and *emcee*. The galaxy

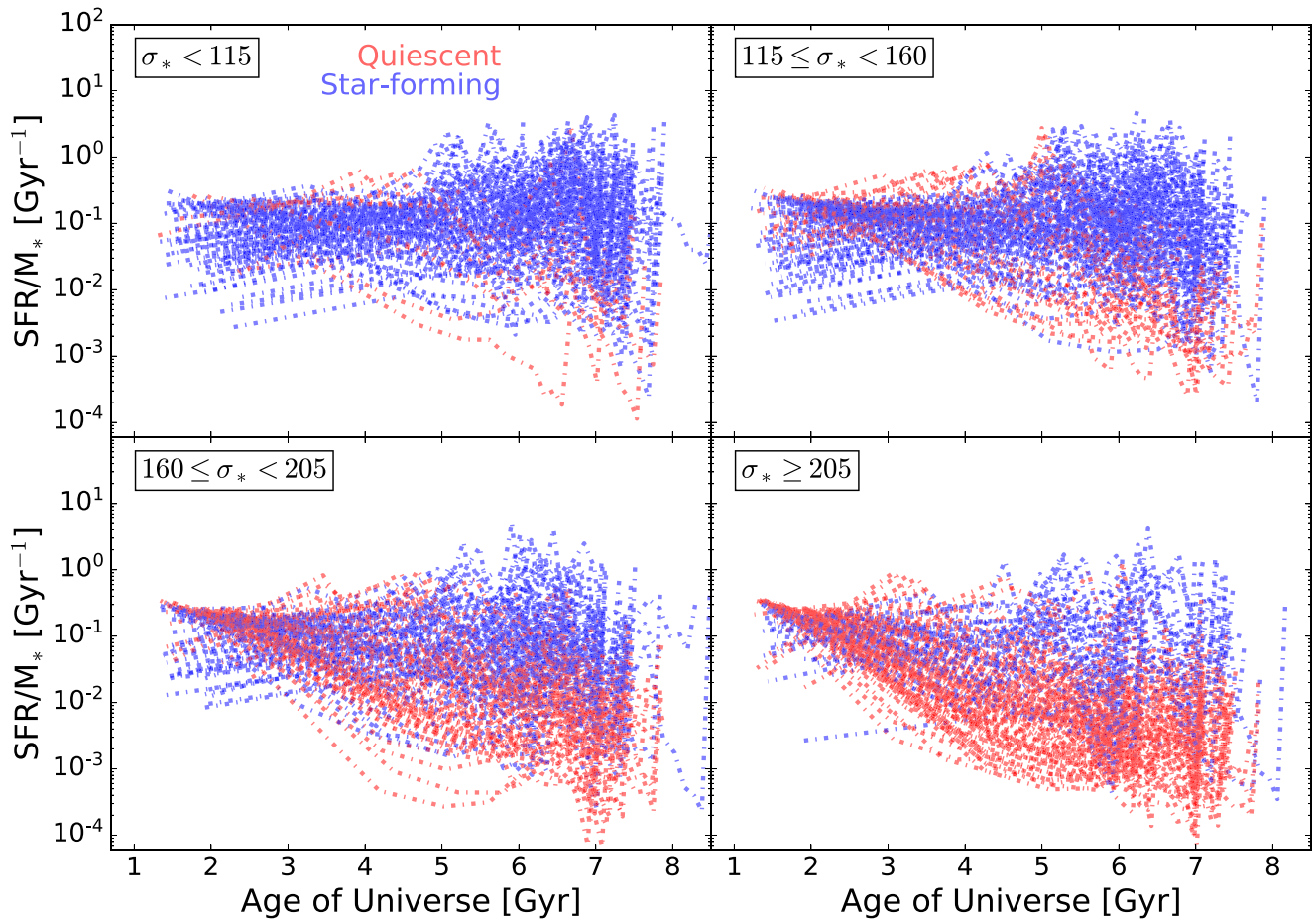


Figure 9. SFHs of the LEGA-C sample (normalized by stellar mass) as a function of the age of the universe separated into four σ_* bins indicated by the labels. The colors differentiate between the star-forming and quiescent populations at the observed redshift.

spectra were fit to a linear combination of a defined set of 12 CSPs, with solar metallicity and constant SF within the time interval of the templates. In 90% of the cases, the algorithm produced good fits based on the normalized χ^2 values. We found a wide variety of SFHs, although 60% of the galaxies have $a_{\langle \text{MW} \rangle} > 3$ Gyr by the time we observe them (Figures 3 and 4). However, we note that age estimates from spectral fits experience increasing degeneracy of spectral features as the stellar populations age. Most of the old galaxies ($a_{\langle \text{MW} \rangle} \gtrsim 3$ Gyr) had very low SFRs early on ($\gtrsim 6$ Gyr after the Big Bang, Figure 4). However, some exhibit subsequent peaks in SF, which could be an indication of rejuvenated SF, or a merger with a younger population. However, the mass formed from this more recent SF activity is only about 10% of the mass formed throughout the galaxies' histories. The median $a_{\langle \text{LW} \rangle}$, $a_{\langle \text{MW} \rangle}$, and $M_{*,\text{FIT}}$ were found to be 1.2 Gyr, 3.8 Gyr, and $10^{10.8} M_{\odot}$, respectively.

The main objective of this work was to investigate how our reconstructed SFHs behave as a function of stellar mass, stellar velocity dispersion, and SF activity, as well as the variation they show at fixed velocity dispersion. We found that galaxies at $z \sim 1$ have similar trends in their SFHs compared to local galaxies, i.e., the stellar content in massive galaxies formed earlier and faster (Figure 8). This top-down scenario is a known trend from fossil record inferences using SDSS spectra; however, in this study, it is shown for $z \sim 1$ galaxies for the first time using full spectrum fitting. We found that the scatter between the quiescent and star-forming populations increases toward lower redshift (Figure 9), which indicates that current

SF activity is strongly correlated with past SF activity. High-dispersion quiescent galaxies had their SF peak early, > 9.5 Gyr ago, and exhibit decreasing SFRs throughout the rest of their history, for the most part. We found that the lowest dispersion galaxies in our sample are undergoing the main stage of their SF as we observe them (7 Gyr ago).










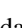




The results of the spectral fits were used to measure a number of galaxy properties, viz. ages ($a_{\langle \text{LW} \rangle}$, $a_{\langle \text{MW} \rangle}$, $a_{\langle \text{MW} \rangle}$, etc.) and stellar mass, in order to test the model by investigating how these properties relate to one another as well as other properties measured from the galaxy spectra, e.g., velocity dispersion, $\text{H}\delta$, D_n4000 , etc. We showed that galaxies evolve from the top left to the bottom right of the $\text{EW}(\text{H}\delta)$ – D_n4000 plane as they age, as would be expected (Figure 5).

Recovering the full SFHs of intermediate-redshift galaxies opens up a multitude of avenues of research. In this work, we have shown the clear differences between the SFHs of quiescent and star-forming galaxies and how these SFHs are scattered at fixed velocity dispersion. We have also shown that velocity dispersion is a better indicator of the age and current SF activity of galaxies as a whole than stellar mass, while stellar mass is a better indicator of the age of star-forming galaxies (Figures 6 and 7). In future studies, we will use the reconstructed SFHs to constrain the quenching speed and rate, as well as investigate the relationship between galactic structure and SFHs. These constraints will become valuable for future surveys like *JWST* that will be investigating the properties of

galaxies beyond $z \sim 2$, and will need $z \sim 1$ measurements as a benchmark to connect those populations to the local universe.

Based on observations made with ESO Telescopes at the La Silla Paranal Observatory under programme ID 194-A.2005 (The LEGA-C Public Spectroscopy Survey). P.C. gratefully acknowledges financial support through a DAAD-Stipendium. This project has received funding from the European Research Council (ERC) under the European Union's Horizon 2020 research and innovation programme (grant agreement No. 683184). K.N. and C.S. acknowledge support from the Deutsche Forschungsgemeinschaft (GZ: WE 4755/4-1). We gratefully acknowledge the NWO Spinoza grant.

ORCID iDs

Priscilla Chauke  <https://orcid.org/0000-0002-1442-984X>
 Arjen van der Wel  <https://orcid.org/0000-0002-5027-0135>
 Camilla Pacifici  <https://orcid.org/0000-0003-4196-0617>
 Rachel Bezanson  <https://orcid.org/0000-0001-5063-8254>
 Po-Feng Wu  <https://orcid.org/0000-0002-9665-0440>
 Anna Gallazzi  <https://orcid.org/0000-0002-9656-1800>
 Caroline Straatman  <https://orcid.org/0000-0001-5937-4590>
 Marijn Franx  <https://orcid.org/0000-0002-8871-3026>
 Eric F. Bell  <https://orcid.org/0000-0002-5564-9873>
 Gabriel B. Brammer  <https://orcid.org/0000-0003-2680-005X>
 Michael V. Maseda  <https://orcid.org/0000-0003-0695-4414>
 Adam Muzzin  <https://orcid.org/0000-0002-9330-9108>
 Hans-Walter Rix  <https://orcid.org/0000-0003-4996-9069>
 David Sobral  <https://orcid.org/0000-0001-8823-4845>

References

- Abramson, L. E., Gladders, M. D., Dressler, A., et al. 2016, *ApJ*, **832**, 7
 Barišić, I., van der Wel, A., Bezanson, R., et al. 2017, *ApJ*, **847**, 72
 Barro, G., Faber, S. M., Koo, D. C., et al. 2017, *ApJ*, **840**, 47
 Belli, S., Newman, A. B., & Ellis, R. S. 2015, *ApJ*, **799**, 206
 Best, P. N., Kauffmann, G., Heckman, T. M., & Ivezić, Ž. 2005, *MNRAS*, **362**, 9
 Bezanson, R., van der Wel, A., Pacifici, C., et al. 2018, *ApJ*, **858**, 60
 Brammer, G. B., Whitaker, K. E., van Dokkum, P. G., et al. 2011, *ApJ*, **739**, 24
 Bruzual, G., & Charlot, S. 2003, *MNRAS*, **344**, 1000
 Calzetti, D., Armus, L., Bohlin, R. C., et al. 2000, *ApJ*, **533**, 682
 Cappellari, M., & Emsellem, E. 2004, *PASP*, **116**, 138
 Chabrier, G. 2003, *PASP*, **115**, 763
 Charlot, S., & Fall, S. M. 2000, *ApJ*, **539**, 718
 Choi, J., Conroy, C., Moustakas, J., et al. 2014, *ApJ*, **792**, 95
 Cid Fernandes, R., Asari, N. V., Sodré, L., et al. 2007, *MNRAS*, **375**, L16
 Cid Fernandes, R., Mateus, A., Sodré, L., Stasińska, G., & Gomes, J. M. 2005, *MNRAS*, **358**, 363
 Cimatti, A., Daddi, E., & Renzini, A. 2006, *A&A*, **453**, L29
 Conroy, C., & Gunn, J. E. 2010, *ApJ*, **712**, 833
 Conroy, C., Gunn, J. E., & White, M. 2009, *ApJ*, **699**, 486
 Diemer, B., Sparre, M., Abramson, L. E., & Torrey, P. 2017, *ApJ*, **839**, 26
 Foreman-Mackey, D., Hogg, D. W., Lang, D., & Goodman, J. 2013, *PASP*, **125**, 306
 Foreman-Mackey, D., Sick, J., & Johnson, B. 2014, python-fsps: Python bindings to FSPS (v0.1.1), Zenodo, doi:10.5281/zenodo.12157
 Franx, M., van Dokkum, P. G., Förster Schreiber, N. M., et al. 2008, *ApJ*, **688**, 770
 Gallazzi, A., Bell, E. F., Zibetti, S., Brinchmann, J., & Kelson, D. D. 2014, *ApJ*, **788**, 72
 Gallazzi, A., Charlot, S., Brinchmann, J., White, S. D. M., & Tremonti, C. A. 2005, *MNRAS*, **362**, 41
 Girardi, L., Bressan, A., Bertelli, G., & Chiosi, C. 2000, *A&AS*, **141**, 371
 Gladders, M. D., Oemler, A., Dressler, A., et al. 2013, *ApJ*, **770**, 64
 Goodman, J., & Weare, J. 2010, *Commun. Appl. Math. Comput. Sci.*, **5**, 65
 Graves, G. J., Faber, S. M., & Schiavon, R. P. 2009, *ApJ*, **698**, 1590
 Heavens, A. F., Jimenez, R., & Lahav, O. 2000, *MNRAS*, **317**, 965
 Ibarra-Medel, H. J., Sánchez, S. F., Avila-Reese, V., et al. 2016, *MNRAS*, **463**, 2799
 Iyer, K., & Gawiser, E. 2017, *ApJ*, **838**, 127
 Jørgensen, I., & Chiboucas, K. 2013, *AJ*, **145**, 77
 Jørgensen, I., Chiboucas, K., Berkson, E., et al. 2017, *AJ*, **154**, 251
 Juneau, S., Glazebrook, K., Crampton, D., et al. 2005, *ApJL*, **619**, L135
 Karim, A., Schinnerer, E., Martínez-Sansigre, A., et al. 2011, *ApJ*, **730**, 61
 Kauffmann, G., Heckman, T. M., White, S. D. M., et al. 2003, *MNRAS*, **341**, 54
 Khostovan, A. A., Sobral, D., Mobasher, B., et al. 2015, *MNRAS*, **452**, 3948
 Koleva, M., Prugniel, P., Bouchard, A., & Wu, Y. 2009, *A&A*, **501**, 1269
 Kriek, M., Conroy, C., van Dokkum, P. G., et al. 2016, *Natur*, **540**, 248
 Kriek, M., van Dokkum, P. G., Labbé, I., et al. 2009, *ApJ*, **700**, 221
 Kroupa, P., Aarseth, S., & Hurley, J. 2001, *MNRAS*, **321**, 699
 Leitner, S. N. 2012, *ApJ*, **745**, 149
 Madau, P., & Dickinson, M. 2014, *ARA&A*, **52**, 415
 Maraston, C., Strömbäck, G., Thomas, D., Wake, D. A., & Nichol, R. C. 2009, *MNRAS*, **394**, L107
 Marigo, P., & Girardi, L. 2007, *A&A*, **469**, 239
 Marigo, P., Girardi, L., Bressan, A., et al. 2008, *A&A*, **482**, 883
 McDermid, R. M., Alatalo, K., Blitz, L., et al. 2015, *MNRAS*, **448**, 3484
 Mosleh, M., Tacchella, S., Renzini, A., et al. 2017, *ApJ*, **837**, 2
 Moustakas, J., Coil, A. L., Aird, J., et al. 2013, *ApJ*, **767**, 50
 Muzzin, A., Marchesini, D., Stefanon, M., et al. 2013a, *ApJ*, **777**, 18
 Muzzin, A., Marchesini, D., Stefanon, M., et al. 2013b, *ApJS*, **206**, 8
 Ocvirk, P., Pichon, C., Lançon, A., & Thiébaud, E. 2006, *MNRAS*, **365**, 46
 Onodera, M., Carollo, C. M., Renzini, A., et al. 2015, *ApJ*, **808**, 161
 Pacifici, C., Kassim, S. A., Weiner, B. J., et al. 2016, *ApJ*, **832**, 79
 Pozzetti, L., Bolzonella, M., Zucca, E., et al. 2010, *A&A*, **523**, A13
 Sánchez-Blázquez, P., Peletier, R. F., Jiménez-Vicente, J., et al. 2006, *MNRAS*, **371**, 703
 Schiavon, R. P., Faber, S. M., Konidaris, N., et al. 2006, *ApJL*, **651**, L93
 Terrazas, B. A., Bell, E. F., Henriques, B. M. B., et al. 2016, *ApJL*, **830**, L12
 Thomas, D., Maraston, C., Bender, R., & Mendes de Oliveira, C. 2005, *ApJ*, **621**, 673
 Thomas, D., Maraston, C., Schawinski, K., Sarzi, M., & Silk, J. 2010, *MNRAS*, **404**, L775
 Toft, S., Gallazzi, A., Zirm, A., et al. 2012, *ApJ*, **754**, 3
 Tojeiro, R., Heavens, A. F., Jimenez, R., & Panter, B. 2007, *MNRAS*, **381**, 1252
 Tojeiro, R., Wilkins, S., Heavens, A. F., Panter, B., & Jimenez, R. 2009, *ApJS*, **185**, 1
 Torrey, P., Wellons, S., Ma, C.-P., Hopkins, P. F., & Vogelsberger, M. 2017, *MNRAS*, **467**, 4872
 van de Sande, J., Kriek, M., Franx, M., et al. 2013, *ApJ*, **771**, 85
 van der Wel, A., Bell, E. F., van den Bosch, F. C., Gallazzi, A., & Rix, H.-W. 2009, *ApJ*, **698**, 1232
 van der Wel, A., Noeske, K., Bezanson, R., et al. 2016, *ApJS*, **223**, 29
 van Dokkum, P. G., & Brammer, G. 2010, *ApJL*, **718**, L73
 Vogelsberger, M., Genel, S., Springel, V., et al. 2014, *MNRAS*, **444**, 1518
 Weisz, D. R., Dalcanton, J. J., Williams, B. F., et al. 2011, *ApJ*, **739**, 5
 Whitaker, K. E., van Dokkum, P. G., Brammer, G., et al. 2013, *ApJL*, **770**, L39
 Whitaker, K. E., van Dokkum, P. G., Brammer, G., & Franx, M. 2012, *ApJL*, **754**, L29
 Wilkinson, D. M., Maraston, C., Thomas, D., et al. 2015, *MNRAS*, **449**, 328
 Wu, P.-F., van der Wel, A., Gallazzi, A., et al. 2018, *ApJ*, **855**, 85
 York, D. G., Adelmann, J., Anderson, J. E., Jr., et al. 2000, *AJ*, **120**, 1579